

RSC Advances



This is an *Accepted Manuscript*, which has been through the Royal Society of Chemistry peer review process and has been accepted for publication.

Accepted Manuscripts are published online shortly after acceptance, before technical editing, formatting and proof reading. Using this free service, authors can make their results available to the community, in citable form, before we publish the edited article. This *Accepted Manuscript* will be replaced by the edited, formatted and paginated article as soon as this is available.

You can find more information about *Accepted Manuscripts* in the [Information for Authors](#).

Please note that technical editing may introduce minor changes to the text and/or graphics, which may alter content. The journal's standard [Terms & Conditions](#) and the [Ethical guidelines](#) still apply. In no event shall the Royal Society of Chemistry be held responsible for any errors or omissions in this *Accepted Manuscript* or any consequences arising from the use of any information it contains.

TiO₂ nanoparticulate-wires hybrids for highly efficient solid-state dye-sensitized solar cells using SSP-PEDOTs

Cite this: DOI: 10.1039/x0xx00000x

Jongbeom Na, Jeonghun Kim, Chihyun Park and Eunkyong Kim*

Received 00th January 2012,
Accepted 00th January 2012

DOI: 10.1039/x0xx00000x

www.rsc.org/

TiO₂ photoanodes for I₂-free solid state dye-sensitized solar cells (ssDSSCs) were prepared from multifunctional new TiO₂ nanostructures to enhance light harvesting and high charge-collection efficiency in ssDSSCs using poly(3,4-ethylenedioxythiophene)s (PEDOTs). A new type of TiO₂ paste containing TiO₂ nanowires (TNW) was prepared and successfully transformed to TiO₂ nanoparticulate-wire hybrids (TNPW) with large surface area of 61.4 m² g⁻¹ through thermal annealing. The thickness of TNPW layer could be controlled up to 17 μm without cracks. As a hole transport material, PEDOTs were infiltrated into the TNPW photoanode through in-situ solid state polymerization (SSP-PEDOTs) and N719 dyes were adsorbed to give ssDSSCs. The SSP-PEDOTs based ssDSSCs with the TNPW photoanodes recorded high cell efficiency (η) of 6.4 % and short-circuit current (J_{sc}) of 14.3 mA cm⁻² without scattering particles, which were 30.6 and 22.2 % higher than those of traditional TiO₂ nanoparticles (TNP) at the same conditions. Furthermore, a liquid-state DSSCs with the TNPW photoanode attained a η of 8.4 %, which was superior to that of a reference TNP cell (7.3 %). The maximum η were obtained as 7.1 and 9.9 % in ssDSSCs and liquid type DSSCs, respectively, in the presence of additional scattering layers, to support the importance of TNPWs. These enhanced photovoltaic performances of TNPW cells could be attributed to the unique TNPW structures that are advantageous for high charge-collection with long electron diffusion path and large surface area needed for high dye adsorption

Introduction

Interfacial charge transport in nanostructured metal oxides for photovoltaic conversion is highly sensitive to their size, shape, and surface structure.¹⁻³ In particular, the charge collection efficiency of a TiO₂ photoanode in DSSCs⁴⁻⁹ is deeply related to the TiO₂ nanostructure,^{10, 11} which could affect more critically to the relatively low efficient solid-state DSSCs (ssDSSCs). The TiO₂ nanoparticles of traditional paste with 10-20 nm size have advantages for efficient dye adsorption resulting in a high photocurrent generation, however, they limit the photoconversion efficiency of a cell because of the high charge recombination resulting from electron trapping events at the interfacial grain boundary of the nanoparticles.¹²⁻¹⁸ To reduce such charge recombination and thus enhance charge transport through the TiO₂ nanostructure, a photoanode with one-dimensional (1D) nanomaterials has been suggested.^{19, 20} Although considerable efforts have been devoted to the fabrication of 1D TiO₂ nanostructures including nanotubes (NTs),²¹⁻²⁴ nanowires (NWs),^{25, 26} and nanorods (NRs),^{27, 28} the relatively low surface area of such a structure limits further enhancement in the photocurrent density.

Recently, liquid-type DSSCs using double-layered photoanode was reported using oriented hierarchical TiO₂ nanowire arrays (HNWs) and nanoparticle (NP). Compared to an NP-based cell, the TiO₂ HNW cell showed a lower electron recombination rate.²⁹ Nevertheless, the photoconversion efficiency (PCE) with the HNW/NP double layer was low, as expected from the limited interfacial electron transport at the NP layer and low dye

adsorption at the HNW layer. Obviously, the HNW/NP double layer system cannot be applied to ssDSSCs, because the efficiency of leak-free ssDSSCs are generally lower than liquid-type DSSCs. Therefore, it remains an important challenge to solve the conflicting problem between the surface area needed for large dye adsorption and 1D nanostructures for long electron transport.

To enhance not only electron transport but also large dye adsorption in 1D nanostructures and ssDSSCs, we propose a facile synthesis of a new TiO₂ nanostructure having a long electron diffusion length, large surface area, and light harvesting property. Compared to other complicated methods^{30, 31} including electrochemical lithography, photoelectrochemical etching, and template synthesis, we explore a paste coating process for the synthesis of 1D metal oxide nanostructures, as it allows precise controllability in the structure within a short reaction time.

The ssDSSCs in this work is based on a I₂-free, solid state conjugated polymer as a hole transporting material, which is grown in situ inside TiO₂ nanopores, as reported before.^{32, 33} As the TiO₂ photoanode based on commercial TiO₂ nanoparticles showed the limitation in increasing short-circuit current density (J_{sc}), open-circuit voltage (V_{oc}), fill factor (FF), and efficiency (η) of ssDSSCs, due to the intrinsic problems of spherical TiO₂ nanoparticles, we explore a new TiO₂ nanostructure for high interfacial charge-collection capacity. Herein we report large scale synthesis of TNW paste and efficient nanostructure of TiO₂ nanoparticulate-wire hybrids (TNPW) for a high performance

photoanode of ssDSSCs possessing a high charge collection capacity and efficient light harvesting.

Experimental

Materials: Ethanol, 1-butanol, isopropyl alcohol, acetonitrile, 1,2-dimethyl-3-propylimidazolium iodide, iodine, *tert*-butylpyridine, lithium iodide, lithium acetate dihydrate (LiAc.2H₂O), acetic acid, anhydrous terpineol, ethyl cellulose, titanium (IV) butoxide, N, N-dimethylformamide (DMF), and titanium bis(ethyl acetoacetate) were purchased from Aldrich. The TiO₂ paste (Dyesol 18NR-T) were purchased from Dyesol, LTD. (Australia) and N719 dye was purchased from Solaronix (Switzerland). All solvents and chemicals were reagent grade and used as received. DBEDOT(2,5-dibromo-3,4-ethylenedioxythiophene) was prepared according to the procedure of our previous report³²

Synthesis of TiO₂ Nanowires: TiO₂ nanowires were synthesized by solvothermal method. Thus 0.2 g of lithium acetate dihydrate and 2 mL of titanium(IV) butoxide (TB) were dissolved in 10 mL of solvent mixture consisting of DMF and acetic acid. The solution was transferred into a Teflon lined stainless steel autoclave, and heated in an oven at 200 °C for 20 h. Finally, the 1D nanowires were collected and washed thoroughly with ethanol for several times, and dried overnight in a vacuum oven at 60 °C.

Preparation of TiO₂ Paste and TNPW Photoanode: As prepared TiO₂ nanowires (5 g) and acetic acid (1 mL) were mixed for 5 min and the mixture was grinded for 5 min after adding 5 mL of deionized water. All liquid reagents were added drop by drop into the grinder. Then, 30 mL of ethanol was added and mixed thoroughly. Excess ethanol (100 mL) was added to the mixture, which was stirred with a rate of 500 rpm. Anhydrous terpineol (17 g) and 28 g of ethyl cellulose solution (10 wt% in ethanol) were added to the above mixture. After stirring, and sonicated, ethanol was removed by rotary evaporator to give TiO₂ nanowire paste. The prepared paste was cast onto a compact TiO₂ layer coated FTO glass using a doctor-blade technique and dried at 70 °C for 1 hr, followed by successive sintering at 450 °C for 30 min and cooling to 30 °C for 8 h. The above conventional compact TiO₂ layer with a 200 nm thickness was prepared by spin coating a titanium bis(ethyl acetoacetate) solution (2 wt% in butanol) onto FTO (Pilkington, 8 Ω⁻¹) glass at 2000 rpm for 30 s, followed by calcination at 450 °C for 30 min. Separately, a commercially available TiO₂ paste (Dyesol 18NR-T) was used to prepare TNP photoanode by the same method for comparison.

Device Fabrication: The prepared photoanodes were immersed in a dye solution containing N719 (0.3 mM in ethanol) for 24 hr at room temperature. The Pt counter electrodes were prepared by drop-casting a H₂PtCl₆ solution (7 mM in isopropyl alcohol) onto a conductive FTO and followed by heating at 400 °C for 20 min, and cooling to 30 °C for 8 hr. The dye adsorbed TiO₂ electrodes and the Pt counter were faced each other as a sandwich-type cell using a hot-melt film (Surlyn, 25 μm) as spacer. The ssDSSCs were fabricated by drop-casting the HTM solution onto the photoanode and covering with a Pt-coated counter electrode. DBEDOT was dissolved in ethanol. Firstly, a few drops of dilute solution (1 wt%) of DBEDOT were dropped onto the TiO₂ photoanodes and dried under ambient conditions. Then a few further drops of more concentrated solution (3 wt%) of DBEDOT in ethanol were directly cast onto the above photoanodes. After evaporating the solvent, the DBEDOT-incorporated photoanodes were thermally polymerized at 55 °C for 24 h in an oven to produce highly conductive polymer channels (Fig. 1c). A drop of the acetonitrile solution consisting of 1-methyl-3-

propyl-imidazolium iodide (1.0 M), 4-*tert*-butylpyridine (0.2 M) and lithium bistrifluoromethanesulfonimide (0.2 M) was coated onto the photoanode as an electrolyte and dried before assembly of ssDSSCs with Pt counter electrode (Fig. 1d). For the preparation of liquid type DSSCs, the acetonitrile solution containing 0.6 M of 1,2-dimethyl-3-propylimidazolium iodide, 0.1 M of iodine, 0.5 M of *tert*-butylpyridine, and 0.1 M of lithium iodide was injected into the cell through a hole in the counter electrode. The active area of the cell was fixed to 0.16 cm².

Characterization: The morphology of TiO₂ was observed by a field emission scanning electron microscope (FE-SEM, JEOL Ltd, model JSM-7001F) and a transmission electron microscope (TEM, JEOL Ltd, model JSM-2010). The X-ray diffraction (XRD) measurement were carried out using a Rigaku (Ultima IV) wide-angle goniometer using Cu-Kα radiation. The optical property (transmittance and reflectance) of TiO₂ film and concentration of dye adsorption were determined by using a UV/Vis spectrophotometer (PerkinElmer, Lambda 750). Photoelectrochemical and photovoltaic characteristics of the TNP and TNPW cells were determined using an electrochemical workstation (Keithley Model 2400) and a solar simulator (1000 W xenon lamp, Oriel, 91193). The light exposure was homogeneous across a 8 × 8 inch² area and was calibrated with a Si solar cell (Fraunhofer Institute for Solar Energy Systems, Mono-Si + KG filter, Certificate No. C-ISE269) to a sunlight intensity of 1 (100 mW cm⁻²). This calibration was confirmed with a NREL-calibrated Si solar cell (PV Measurements Inc.). IMVS and IMPS measurement were carried out on an electrochemical workstation equipped with a frequency response analyzer under a modulated green light-emitting diode (535 nm) driven by a source supply, which could provide both DC and AC illumination components (frequency range : from 10000 to 0.01 Hz). IPCE spectra were obtained as a function of wavelength from 300 to 800 nm. The amount of adsorbed dye was determined by measuring dye desorption after immersion of the dye adsorbed TiO₂ film into a solution of NaOH (5 mM) in an ethanol/water (1:2 v/v) mixture. The concentration of the desorbed dye was analyzed by using a UV/Vis spectrophotometer.

Results and discussion

A superior photoanode with TNPW was prepared from a paste composed of TiO₂ nanowires (TNWs) and through the thermal treatment. The TNWs were synthesized by a simple solvothermal reaction in DMF and acetic acid according to the previously described method³⁴ (Fig. 1a). The pristine TNWs were obtained in a large-scale with an average diameter of ~15 nm and several hundred nanometer in length as shown in Fig. 2a-b. A new paste containing the TNWs was prepared as a viscous yellowish solution, which was coated onto a FTO substrate that was pre-coated with a 200 nm thick compact TiO₂ layer.^{32, 35} Upon calcination at ~450 °C for 30 min, the thin TNWs were aggregated and popped-up to yield TNPW, as shown in Fig. 2c, g. On the other hand, the nanowire structures were maintained when calcined at a mild condition of 350 °C for 2 h. The length and diameter of the TNPW were approximately 200 nm and 40 nm, respectively, which were larger than those of the TiO₂ nanoparticles from the common paste. The reformation of TNPW could be attributed to aggregation and shrinkage of TNW bundle at high temperature (450 °C) as schematically shown in Fig. S1a. It is noteworthy that a 17 μm-thick, large-area (3 cm × 2 cm) TNPW photoanode could be prepared without cracks from the TNWs paste. Moreover, the TNPW photoanodes showed a dense and well-organized mesoporous structure, as shown in Fig. S2. than those of the TiO₂ nanoparticles from the common paste. The reformation of

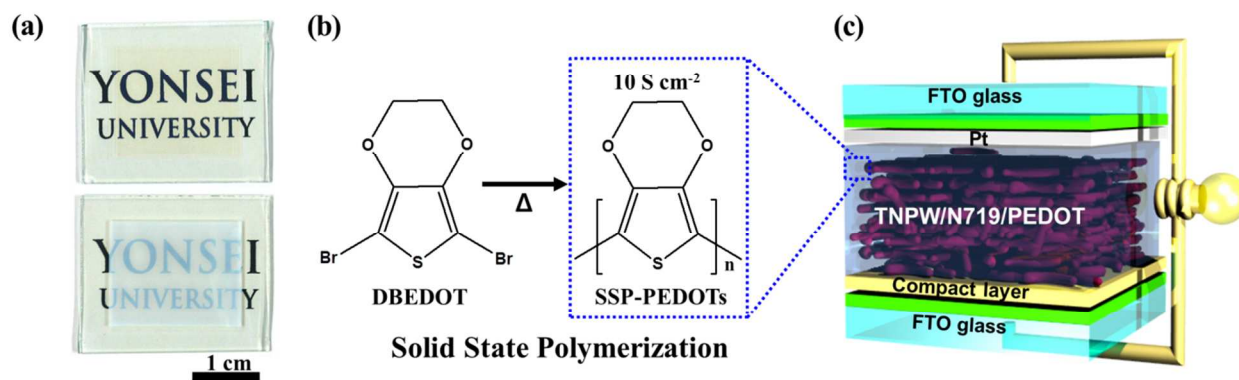


Fig. 1. (a) Photographic images of the coated and calcined photoanodes on FTO using commercial TiO₂ nanoparticle paste (top) and TNWs paste (bottom). (b) The chemical structures of DBEDOT and solid-state-polymerized PEDOTs with 10 S cm⁻¹. (c) Schematic representation of the ssDSSCs structure that fabricated with TNPW/N719 dye photoanode.

TNPW could be attributed to aggregation and shrinkage of TNW bundle at high temperature (450 °C) as schematically shown in Fig. S1a. It is noteworthy that a 17 μm-thick, large-area (3 cm x 2 cm) TNPW photoanode could be prepared without cracks from the TNWs paste. Moreover, the TNPW photoanodes showed a dense and well-organized mesoporous structure, as shown in Fig. S2. The high resolution TEM (HR-TEM) images for the pristine TNWs (Fig. 2d-i) show a typical continuous lattice fringe of anatase TiO₂

with lattice spacings of 0.35 nm, which corresponded to the (101) crystalline plane. The phase purity and structure of pristine TNWs were examined further by X-ray diffraction (XRD) analysis in the 2θ range of 20 ° to 60 ° (Fig. S1b). The sharp peaks at 25.3, 36.9, 37.8, 38.5, 47.9, 53.9, and 55 ° correspond to the reflections from the (101), (103), (104), (112), (200), (105), and (211) crystal planes of anatase TiO₂, respectively (JCPDS No.21-1272).

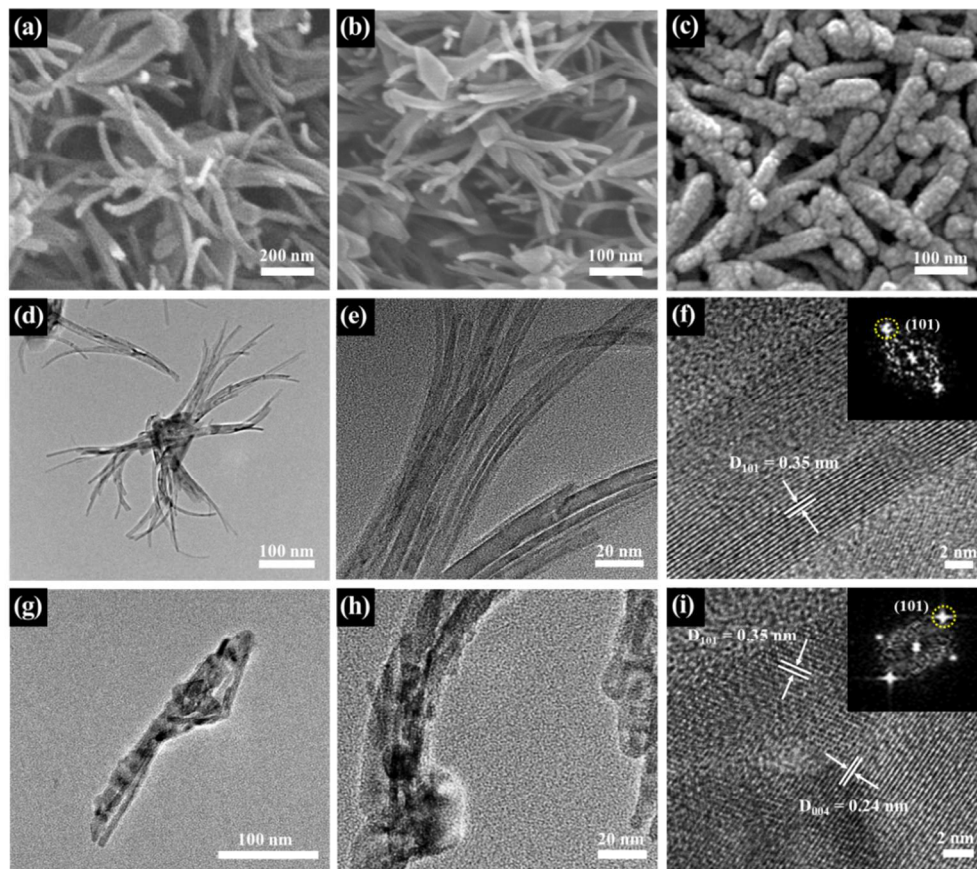


Fig. 2. SEM images of TiO₂ nanostructures. (a) after synthesis, (b) after annealing at 350 °C for 2 h and (c) after calcination of TNWs paste at 450 °C. TEM image of (d),(e) TNWs, (g),(h) TNPW and magnified HRTEM image of (f) TNWs, (i) TNPW corresponding Fourier transform (FFT) pattern (inset).

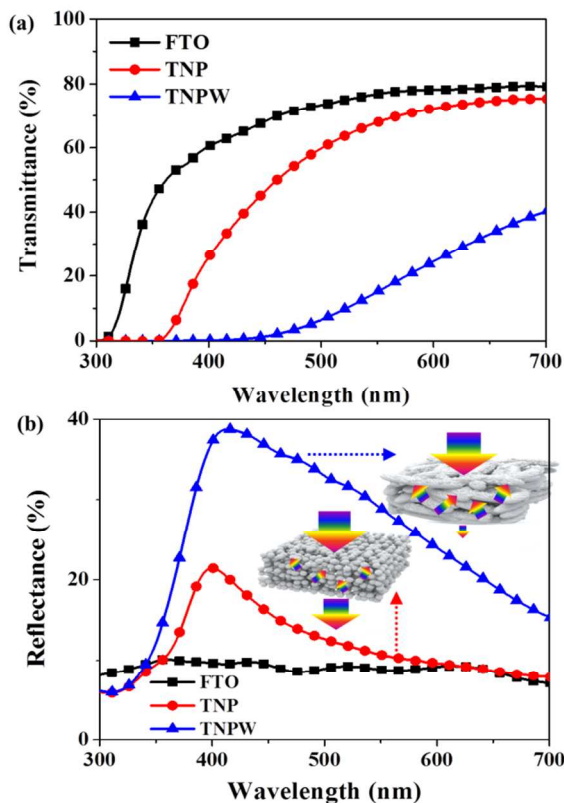


Fig. 3. Optical Properties of TNP and TNPW photoanode. (a) comparison of the transmittance spectra of bare FTO glass (black), TNP (red) and TNPW (blue) film on FTO glass, (b) reflectance spectra of bare FTO, TNP and TNPW films on the FTO substrate with TiO_2 thickness of $10 \mu\text{m}$ for all films. Inset: schematic representation of light trapping by scattering on the TNP and TNPW film.

The lattice spacing of (101) crystalline plane in HR-TEM (Fig. 2f) for the TNWs was well matched to that from XRD. The TNPW were shorter in length but thicker than TNW bundles as compared in Fig. 2. Importantly, the continuous fringes that corresponded to the (101) planes in TNWs (Fig. 2f) were observed in TNPW (Fig. 2i). Moreover, the TNPW showed the same XRD diffraction pattern as that of TNWs (Fig. S1b), indicating that TNPW possess crystal planes of anatase TiO_2 in spite of high temperature treatment. This result suggests that the TNPW layer could be promising as a photoanode, by virtue of the popped-up particle structures to increase surface area and the tightly connected 1D TiO_2 structures useful for the extension of the electron transport path. Light harvesting is one of the important properties for improving cell efficiency in solar cells by maximizing the absorption of incident sun-light.³⁶ As a light harvesting technique, light scattering by larger nanoparticles ($\sim 100 \text{ nm}$)³⁷, light-trapping nanopatterned surface³³ and plasmon light harvesting^{38,39} are commonly incorporated into solar cells. In particular, it has been necessary to add light-scattering layers into DSSCs. This requires extra engineering for the paste composition, such as careful control of the composition as well as distribution of the scattering particles, given that light scattering depends strongly on the size of the particles and the wavelength of the incident light. Because the size of the TNPW ($\sim 200 \text{ nm}$ long and 40 nm wide) are larger than common TNP, the photoelectrode of the

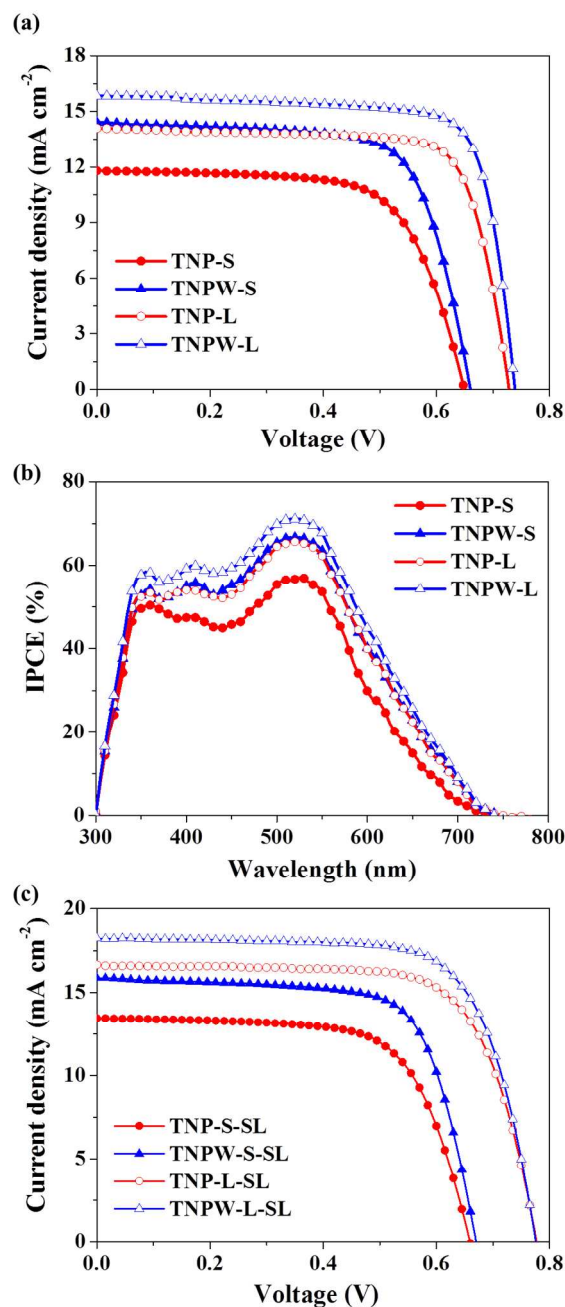


Fig. 4. Cell performances and IPCE results. (a) J - V curves and (b) IPCE for ssDSSCs (filled) and liquid DSSCs (empty) with TNP (red) and TNPW (blue) without scattering layer at 100 mW cm^{-2} . (c) J - V curves of DSSCs with addition of scattering layer at 100 mW cm^{-2}

former exhibits a much higher reflectance compared to that of TNP, as compared in Fig. 3b and Fig. 1b. The high optical reflectance of TNPW was clearly observed in the visible-light wavelength range; that was 2-fold larger in the entire visible range of 400 to 700 nm, compared to the TNP. The increased reflectance was sufficiently large to enhance light harvesting, improving the photocurrent density of DSSCs. Due to their aggregated 1D structures, the TNPW photoanodes exhibit a bit smaller dye adsorption than the TNP, as expected from the smaller surface area of the TNPW (Table S1). On

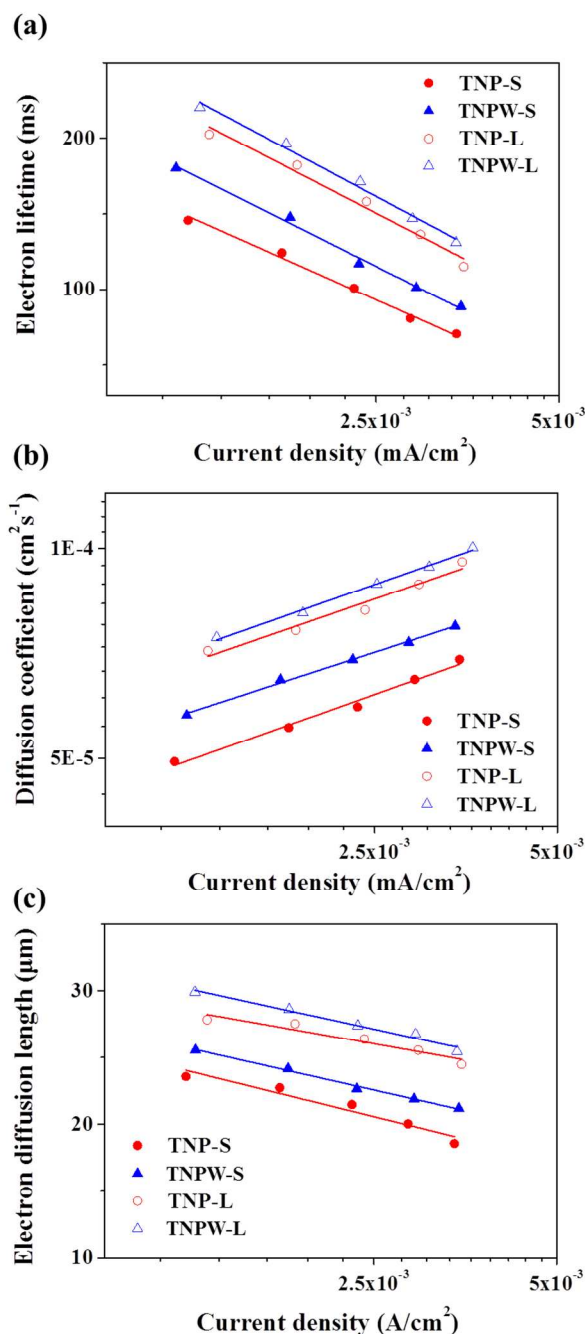


Fig. 5. (a) The electron lifetime (τ_r) and (b) diffusion coefficient (D_n) and (c) electron diffusion length of ssDSSCs (filled) and liquid type DSSCs (empty) fabricated with the TNP (red) and TNPW (blue) as determined from the IMPS / IMVS measurements.

the other hands, the light harvesting properties from the TNPW photoanode was much enhanced as compared with that from the TNP as described below. also higher V_{oc} and FF . This enhancement could be originated from the molecular contact between the hole transport PEDOTs with the dye-adsorbed TNPW which are long enough for extended charge transport and large enough for effective light harvesting. The reflectance of TNPW was much greater than that of TNP. Thus, the TNPW was more effective in utilizing the light absorption of dyes in a photoanode, through enhanced light-

scattering effects at visible regions, resulting in the improvement of current density. This result was consistent with the IPCE data. The IPCE spectra in Fig. 4b show that the quantum efficiency was improved in the visible wavelength region, mainly due to the light harvesting property of TNPW. For TNPW with PEDOTs, the cell efficiency was increased by 30.6 %, probably due to the increase in J_{sc} according to the reflectance increase. Furthermore, the recombination of electrons was prevented much as the long length of TNPW, which could provide good interconnectivity and deep penetration of DBEDOT. Efficiency was increased up to 6.4 % with TNPW, which is among the highest values for N719-dye-based ssDSSCs, and was greater than those of ssDSSCs with TNP.⁴⁰ The electron transport and charge recombination time for the DSSCs were estimated from the intensity-modulated photocurrent spectroscopy (IMPS)/intensity-modulated photovoltage spectroscopy (IMVS) (Fig. 5c,d), according to equations (1) and (2):

$$\tau_d = 1/2\pi f_{dmin} \quad (1)$$

$$\tau_r = 1/2\pi f_{rmin} \quad (2)$$

where f_d (f_r) is the characteristic frequency at the minimum of the IMPS and IMVS imaginary component, and τ_d (τ_r) is the electron transport time (recombination time).⁴¹ The electron lifetime (τ_r) of the TNPW is always longer than those of the TNP cells (Fig. 5c). Such a long τ_r of the TNPW can be attributed to their unique structures (Fig. 2c, and 2g-i): Inside the shape-transformed structures, the aggregated and shrunk TNWs are interconnected extensively, forming long charge transport path (Fig. 5b and S1a). This could reduce the charge recombination at the grain boundary and interface, compared to the spherical nanoparticles (diameter of ~20 nm) with many gaps between the particles. Moreover, TNPW possess smaller surface area than the TNP, reducing the interfacial electron trapping sites for recombination with I^{3-} in the electrolyte, compared to the As shown in Fig. 4 and Table 1, the $J-V$ curve of the ssDSSC fabricated with TNPW and SSP-PEDOTs showed a J_{sc} of 14.3 mA cm⁻² and η of 6.4 %, which were much greater than those of the ssDSSCs with TNP.³² The TNPW photoanode showed not only higher J_{sc} but TNP. As a result, V_{oc} is increased in the TNPW than in the TNP (Table 1). This provides evidence that electrons in the TNPW are prevented more from the interfacial electron recombination with redox species, yielding a high V_{oc} . Furthermore, the electron

diffusion coefficient (D_n) of the TNPW was higher than that of the TNP, as determined from equation (3):

$$D_n = d^2 / (2.35 \tau_d) \quad (3)$$

where d is the thickness of the photoanode.⁴² This indicates a fast electron transport in TNPW because of their well-organized 1 D nanostructure (Fig. 5d). This, in turn, enhances charge-collection capacity, resulting in an increase of the J_{sc} at the same dye adsorption level as the TNP. The effective electron-diffusion length (L_n) was determined from D_n and τ_r using Equation (4) as follows:

$$L_n = (D_n \tau_r)^{1/2} \quad (4)$$

where L_n is the average distance of the injected electrons through the photoanode before recombination.⁴¹ The diffusion length of the TNPW was longer than that of the TNP, therefore, led to higher charge collection efficiency and enhanced current density (Fig. S3). With such high D_n , τ_r , and superior light scattering property, the TNPW photoanodes provide high open-circuit voltage, short-circuit

current, and photoconversion efficiency, despite the low dye loading of the TNPW cell compared to the TNP cell. Moreover, the TNPW

Table 1. Performances of the DSSCs fabricated with various semiconductor nanoparticles at 100 mW cm⁻².

Sample ^{a)}	Thickness	HTM	J_{sc} (mA cm ⁻²)	V_{oc} (V)	FF	η (%)	Dye loading ^{c)} (nmol cm ⁻²)
TNP-S ^{b)}	10 μ m	PEDOTs	11.7	0.65	0.65	4.9	71.4
TNPW-S ^{b)}	10 μ m	PEDOTs	14.3	0.66	0.67	6.4	60.8
TNP-L ^{c)}	11 μ m	Γ / Γ^{3-}	14.1	0.73	0.72	7.3	78.3
TNPW-L ^{c)}	11 μ m	Γ / Γ^{3-}	15.6	0.74	0.73	8.4	67.1
TNP-S-SL ^{b), d)}	8+3 μ m	PEDOTs	13.5	0.66	0.65	5.8	61.2
TNPW-S-SL ^{b), d)}	8+3 μ m	PEDOTs	15.8	0.67	0.67	7.1	54.1
TNP-L-SL ^{c), d)}	11+4 μ m	Γ / Γ^{3-}	16.6	0.77	0.69	8.9	78.9
TNPW-L-SL ^{c), d)}	11+4 μ m	Γ / Γ^{3-}	18.2	0.77	0.70	9.9	68.3
TNP-S / ref 1 ⁴³	-	PPP-b-P3HT	8.8	0.81	0.65	4.65	-
TNP-S / ref 2 ³²	11 μ m	PEDOTs	14.2	0.64	0.60	5.4	-
TNP-S / pat / ref 3 ³³	11 μ m	PEDOTs	19.2	0.65	0.56	7.03	-

^{a)} The devices were fabricated with a transparent TiO₂ layer without a scattering layer. The cells were investigated with metal mask an area of 0.16 cm². ^{b)} The devices of I₂-free ssDSSCs were fabricated with conducting polymer (PEDOTs) as HTM, and ^{c)} I₂ based DSSCs. All devices with N719 dye. ^{d)} The devices were fabricated with scattering layer. Note: TNP devices were prepared from commercially available Dyesol paste.

cell showed higher photoconversion efficiency than the TNWs/TNP double layer system²⁹, possibly due to their unique structure favorableness for fast charge transport plus light scattering structure. The application potential of TNPW was examined in ssDSSCs containing scattering layer (SL) and even in a liquid type DSSC. As shown in Fig. 4 and Table 1, the J - V curve of the ssDSSC fabricated with SL and SSP-PEDOTs showed a J_{sc} of 15.8 mA cm⁻² and η of 7.1 %, which were much greater than those of the ssDSSCs with TNP.^{32,33} Furthermore, liquid type DSSC with TNPW and SL showed a J_{sc} of 18.2 mA cm⁻² and η of 9.9 %. These result strongly indicates that the TNPW is useful not only in the solid type DSSCs but also liquid type cells.

Conclusions

Shape-transformable TiO₂ nanowires (TNWs) semiconductor were synthesized in large scale and used as a new paste to yield superior TNPW photoanodes with well-connected popped-up 1 D structure without cracks, even for a 17 μ m thick film. The TNPW photoanodes have a relatively high surface area (61.4 m² g⁻¹), which is comparable to the TNP. Their combined characteristics of fast charge transport and light harvesting structures provided ssDSSCs of N719 with high V_{oc} (0.66 V) and J_{sc} (14.3 mA). These resulted in a high η of 6.4 %, representing a 30.6 % improvement in efficiency compared to the TNP at the same thickness, respectively. Given the

prominent properties of TNPW, the η of a TNPW liquid state cell reached up to 8.4 % which was higher than those of TNP at the same thickness. In the presence of scattering layers the ssDSSCs showed maximum η of 7.1 %, indicating that TNPW photoanode could be further optimized by the addition of SL. Moreover TNPW photoanode could be applied in liquid type DSSCs, to show a η of 9.9 %. These higher efficiencies could be attributed to the enhanced J_{sc} and V_{oc} values originated from the interconnected TNPW structure with large pores and high porosity, which are effective for both high dye adsorption and long charge transport. The new type of TNPW semiconductor structure with a relatively high surface area, efficient light harvesting, and long electron diffusion paths can be a possible candidate for quantum dot and perovskite solar cells in near future and other optoelectronic devices with high performance.

Acknowledgements

We acknowledge the financial support of National Research Foundation of Korea(NRF) grant funded by the Korea government(MSIP) (No. 2007-0056091).

※ MSIP: Ministry of Science, ICT & Future Planning

Notes and references

Department of Chemical and Biomolecular Engineering, Yonsei University, 50 Yonsei-ro, Seodaemun-gu, Seoul 120-749, Korea.

†J. Na and J. Kim contributed equally to this work.

Electronic Supplementary Information (ESI) available: Detail data of SEM image of TNPW film, surface area, pore volume and pore diameter result of devices. See DOI: 10.1039/b000000x/

- 1 J.-G. Yu, H.-G. Yu, B. Cheng, X.-J. Zhao, J. C. Yu and W.-K. Ho, *J. Phys. Chem. B*, 2003, **107**, 13871-13879.
- 2 Z.-H. Lin, Y. Xie, Y. Yang, S. Wang, G. Zhu and Z. L. Wang, *ACS Nano*, 2013, **7**, 4554-4560.
- 3 S. Seo, C. Allain, J. Na, S. Kim, X. Yang, C. Park, J. Malinge, P. Audebert and E. Kim, *Nanoscale*, 2013, **5**, 7321-7327.
- 4 B. Oregan and M. Gratzel, *Nature*, 1991, **353**, 737-740.
- 5 L. Passoni, F. Ghods, P. Docampo, A. Abrusci, J. Martí-Rujas, M. Ghidelli, G. Divitini, C. Ducati, M. Binda, S. Guarnera, A. Li Bassi, C. S. Casari, H. J. Snaith, A. Petrozza and F. Di Fonzo, *ACS Nano*, 2013, **7**, 10023-10031.
- 6 M. Stefiik, F. J. Heiligtag, M. Niederberger and M. Grätzel, *ACS Nano*, 2013, **7**, 8981-8989.
- 7 P.-Y. Chen, X. Dang, M. T. Klug, J. Qi, N.-M. Dorval Courchesne, F. J. Burpo, N. Fang, P. T. Hammond and A. M. Belcher, *ACS Nano*, 2013, **7**, 6563-6574.
- 8 P.-Y. Chen, R. Ladewski, R. Miller, X. Dang, J. Qi, F. Liau, A. M. Belcher and P. T. Hammond, *J. Mater. Chem. A*, 2013, **1**, 2217-2224.
- 9 G. M. Lowman and P. T. Hammond, *Small*, 2005, **1**, 1070-1073.
- 10 J. Nissfolk, K. Fredin, A. Hagfeldt and G. Boschloo, *J. Phys. Chem. B*, 2006, **110**, 17715-17718.
- 11 M. Grätzel, *Inorg. Chem.*, 2005, **44**, 6841-6851.
- 12 N. Kopidakis, K. D. Benkstein, J. van de Lagemaat and A. J. Frank, *J. Phys. Chem. B*, 2003, **107**, 11307-11315.
- 13 A. Solbrand, A. Henningsson, S. Södergren, H. Lindström, A. Hagfeldt and S.-E. Lindquist, *J. Phys. Chem. B*, 1999, **103**, 1078-1083.
- 14 D. K. Roh, W. S. Chi, S. H. Ahn, H. Jeon and J. H. Kim, *ChemSusChem*, 2013, **6**, 1384-1391.
- 15 J. Qu, G. R. Li and X. P. Gao, *Energy Environ. Sci.*, 2010, **3**, 2003-2009.
- 16 M. J. Bierman and S. Jin, *Energy Environ. Sci.*, 2009, **2**, 1050-1059.
- 17 L. Hu, S. Dai, J. Weng, S. Xiao, Y. Sui, Y. Huang, S. Chen, F. Kong, X. Pan, L. Liang and K. Wang, *J. Phys. Chem. B*, 2007, **111**, 358-362.
- 18 T. Berger, T. Lana-Villarreal, D. Monllor-Satoca and R. Gómez, *J. Phys. Chem. C*, 2007, **111**, 9936-9942.
- 19 F. Shao, J. Sun, L. Gao, S. Yang and J. Luo, *J. Mater. Chem.*, 2012, **22**, 6824-6830.
- 20 J.-Y. Liao, B.-X. Lei, H.-Y. Chen, D.-B. Kuang and C.-Y. Su, *Energy Environ. Sci.*, 2012, **5**, 5750-5757.
- 21 M. Ye, D. Zheng, M. Lv, C. Chen, C. Lin and Z. Lin, *Adv. Mater.*, 2013, **25**, 3039-3044.
- 22 T.-S. Kang, A. P. Smith, B. E. Taylor and M. F. Durstock, *Nano Lett.*, 2009, **9**, 601-606.
- 23 D. K. Roh, W. S. Chi, H. Jeon, S. J. Kim and J. H. Kim, *Adv. Funct. Mater.*, 2014, **24**, 379-386.
- 24 T. Stergiopoulos, E. Rozi, R. Hahn, P. Schmuki and P. Falaras, *Adv. Energy Mater.*, 2011, **1**, 569-572.
- 25 X. Feng, K. Zhu, A. J. Frank, C. A. Grimes and T. E. Mallouk, *Angew. Chem.*, 2012, **124**, 2781-2784.
- 26 X. Feng, K. Shankar, O. K. Varghese, M. Paulose, T. J. Latempa and C. A. Grimes, *Nano Lett.*, 2008, **8**, 3781-3786.
- 27 L. De Marco, M. Manca, R. Giannuzzi, M. R. Belviso, P. D. Cozzoli and G. Gigli, *Energy Environ. Sci.*, 2013, **6**, 1791-1795.
- 28 B. Liu and E. S. Aydil, *J. Am. Chem. Soc.*, 2009, **131**, 3985-3990.
- 29 W.-Q. Wu, J.-Y. Liao, H.-Y. Chen, X.-Y. Yu, C.-Y. Su and D.-B. Kuang, *J. Mater. Chem.*, 2012, **22**, 18057-18062.
- 30 S. Z. Chu, S. Inoue, K. Wada, S. Hishita and K. Kurashima, *J. Electrochem. Soc.*, 2005, **152**, B116-B124.
- 31 P. Hoyer, *Langmuir*, 1996, **12**, 1411-1413.
- 32 J. K. Koh, J. Kim, B. Kim, J. H. Kim and E. Kim, *Adv. Mater.*, 2011, **23**, 1641-1646.
- 33 J. Kim, J. K. Koh, B. Kim, J. H. Kim and E. Kim, *Angew. Chem., Int. Ed.*, 2012, **51**, 6864-6869.
- 34 H. B. Wu, H. H. Hng and X. W. Lou, *Adv. Mater.*, 2012, **24**, 2567-2571.
- 35 J. Kim, J. K. Koh, B. Kim, S. H. Ahn, H. Ahn, D. Y. Ryu, J. H. Kim and E. Kim, *Adv. Funct. Mater.*, 2011, **21**, 4633-4639.
- 36 M. D. Kelzenberg, S. W. Boettcher, J. A. Petykiewicz, D. B. Turner-Evans, M. C. Putnam, E. L. Warren, J. M. Spurgeon, R. M. Briggs, N. S. Lewis and H. A. Atwater, *Nat. Mater.*, 2010, **9**, 239-244.
- 37 J.-W. Shiu, C.-M. Lan, Y.-C. Chang, H.-P. Wu, W.-K. Huang and E. W.-G. Diau, *ACS Nano*, 2012, **6**, 10862-10873.
- 38 J. Qi, X. Dang, P. T. Hammond and A. M. Belcher, *ACS Nano*, 2011, **5**, 7108-7116.
- 39 X. Dang, J. Qi, M. T. Klug, P.-Y. Chen, D. S. Yun, N. X. Fang, P. T. Hammond and A. M. Belcher, *Nano Lett.*, 2013, **13**, 637-642.
- 40 S. Hore, P. Nitz, C. Vetter, C. Prah, M. Niggemann and R. Kern, *Chem. Commun.*, 2005, **15**, 2011-2013.
- 41 K. Yan, Y. Qiu, W. Chen, M. Zhang and S. Yang, *Energy Environ. Sci.*, 2011, **4**, 2168-2176.
- 42 L. Dloczik, O. Ileperuma, I. Lauerma, L. M. Peter, E. A. Ponomarev, G. Redmond, N. J. Shaw and I. Uhlendorf, *J. Phys. Chem. B*, 1997, **101**, 10281-10289.
- 43 W. Chen, Y. Lee, C. Chen, K. Kau, L. Lin, C. Dai, C. Wu, K. Ho, J. Wang and L. Wang, *ACS Nano*, 2014, **8**, 1254-1262